Title

Physical modeling of coupled heat transfer and water flow in soil-borehole thermal energy storage systems in the vadose zone

Authors

Başer, Tuğçe
Traore, Thierry
McCartney, John S

Publication Date

2016-03-01

DOI

10.1130/2016.2519(06)

Peer reviewed

Physical Modeling of Coupled Heat Transfer and Water Flow in Soil-Borehole Thermal Energy Storage Systems in the Vadose Zone

Tuğçe Başer[1], Thierry Traore[2], and John S. McCartney[3]

[1]Graduate Research Assistant, Department of Structural Engineering, University of California San Diego, 9500 Gilman Dr. La Jolla, CA 92093-0085. tbaser@ucsd.edu.

[2]Staff Engineer, Brierley and Associates, Denver, CO. ttraore@brierleyassociates.com.

[3]Associate Professor, Department of Structural Engineering, University of California San Diego, 9500 Gilman Dr. La Jolla, CA 92093-0085. mccartney@ucsd.edu.

ABSTRACT

This paper focuses on characterization of the heat transfer and water flow processes in physical models of borehole heat exchanger arrays in unsaturated soil layers. The overall goal is to develop a dataset that can be used to validate coupled thermo-hydraulic flow models needed to simulate the efficiency of heat transfer in soil-borehole thermal energy storage (SBTES) systems. Two bench-scale physical models that consist of a triangular array of vertical heat exchangers within a layer of unsaturated silt were constructed in insulated cylindrical tanks to evaluate the impact of different boundary conditions on the heat transfer and water flow processes in the silt during heat injection into the array. In one model, the heat exchangers were placed at a radial location that is 26% of the tank radius, while in the other model the heat exchangers were placed on the inside of the tank wall. During circulation of heated fluid through the heat exchangers, the changes in soil temperature and volumetric water content along the centerline of the array at different depths were measured using dielectric sensors. The thermal conductivity and specific heat capacity of the silt were also monitored using a thermal probe at the center of the silt layer at mid-height. Permanent drying was observed for the soil within the array with the smaller spacing, while an increase in water content was observed in the array with a spacing equal to the container diameter. An increase in thermal conductivity of the soil was observed within the array in the case of larger spacing, while the opposite was observed in the case of the smaller spacing. The results indicate the possible formation of a convective cell within the larger array as water is driven inwards from the heat exchangers. They indicate the importance of couple heat transfer and water flow in SBTES systems in the vadose zone.

Keywords: Borehole thermal energy storage, Coupled heat transfer and water flow, Laboratory physical modeling, Unsaturated soil

INTRODUCTION

Soil-borehole thermal energy storage (SBTES) systems are an approach to provide efficient renewable resource-based thermal energy to heat buildings (Gabrielsson et al. 2000; Sibbitt et al. 2007; Zhang et al. 2012; McCartney et al. 2013). They function similar to conventional ground-source heat pump (GSHP) systems, where fluid is circulated within a closed-loop pipe network installed in vertical boreholes to shed or absorb heat from the surrounding subsurface. Different from conventional GSHP system, SBTES systems are configured to store thermal energy collected from solar thermal panels during the summer, and discharge the heat to buildings during the winter. The temperature of the ground within the array increases from its ambient temperature (approximately 10-20 °C) to 60-90 °C during heat injection due to thermal inertia of the soil. The maximum temperature a soil can reach is governed by volumetric heat capacity of the soil. A higher value of the volumetric heat capacity implies a longer time for the system to reach equilibrium. SBTES systems are a convenient alternative to other energy storage systems as they are relatively inexpensive, involve storage of renewable energy (solar thermal energy), and are space efficient as they are underground.

One challenge with SBTES systems is the need to improve the efficiency of heat transfer into and out of the array of geothermal boreholes. Zhang et al. (2012) analyzed the heat exchange processes at the Drake Landing site, an example of a successful SBTES project in Alberta, Canada, and found that the efficiency of heat transfer (defined as the amount of heat extracted divided by the amount of heat injected) is approximately 27%. Although the efficiency of heat transfer is low, the SBTES system at the Drake Landing site has provided more than 90% of the heating to 52 houses over the past several years (Sibbitt et al. 2007; 2012). This is an important point to consider as the thermal energy being stored in the SBTES system is obtained freely from a renewable source with a low cost.

An opportunity to enhance the efficiency of SBTES systems is to install them in the vadose zone (the unsaturated zone of soil above the water table). It has been shown that the latent heat of phase change enhances the heat transfer process in unsaturated soil layers, and that convection plays a major role in transporting thermal energy in unsaturated soils subject to a temperature gradient (Cass et al. 1984). In the case of SBTES systems in the vadose zone, it is possible to take advantage of phase change phenomena in the pore water to obtain greater heat injection and extraction rates by formation of a convective cell between the borehole heat exchangers. A convection cell will form in an unsaturated soil layer because as the pore water around the heat exchanger array is heated, it will vaporize and move upward due to buoyancy and toward colder regions away from the heat source. The water then condenses at a cold boundary, releasing latent energy. The water will then flows downward due to gravity and back toward the dry soil around the heat source in response to the suction gradient. During this flow process, enhanced heat transfer will occur when latent energy is absorbed by the water during vaporization and released during condensation. The mechanisms of heat transfer and water flow in the analogous convective cell expected within a borehole heat exchanger array is shown in 2-dimensions in Figure 1. Sakaguchi et al. (2009) observed the formation of a convective cell in an unsaturated soil layer and observed an increase in apparent thermal conductivity with increasing temperature and explained this increase in terms of the latent heat transfer processes occurring in the soil. Lu (2001) found that the rate of heat transfer in a convective cell in an unsaturated soil layer may be up to 10 times faster than assuming that heat conduction is the only mode of heat transfer.

An example of the possible heat transfer and water flow processes associated with the formation of a convective cell within the context of the boundary conditions of an SBTES installed in the vadose zone is shown in Figure 2. The SBTES system incorporates an insulated hydraulic barrier at the soil surface, which is necessary as the long-term performance of the SBTES system may be affected by upward water loss from within the borehole array due to evaporation and thermally-induced water flow. Downward heat flow into the soil below the water table is not restricted, but the lower thermal conductivity of the unsaturated soil outside of the array may provide an insulating effect to help retain heat within the array.

To better understand the behavior of SBTES systems in the vadose zone, the impacts of latent and sensible heat transfer associated with phase change and flow of pore water on the transfer and storage of heat within a geothermal borehole array in an unsaturated silt layer are investigated in this study. Specifically, physical models consisting of a layer of unsaturated silt compacted atop a layer of saturated sand in an insulated, cylindrical tank were constructed to observe these processes during heat injection. Three steel "U"-tube pipes were inserted through the silt layer into the top of the sand layer to simulate an array of geothermal borehole heat exchangers. In one model, the heat exchangers were placed at a radial location that is 26% of the tank radius, while in the other model the heat exchangers were placed on the inside of the tank wall.

During the tests, heated fluid was circulated through the steel pipes to inject heat into the silt layer at a constant rate. The boundary conditions in the test are selected to simulate the behavior of the soil between the borehole array shown in Figure 2, knowing that the lateral heat loss and water transfer out of the array were not properly simulated in the array with the heat exchangers on the inside of the container wall. Sensors to monitor changes in temperature, volumetric water content and thermal conductivity were placed in the silt layer at strategic locations to monitor the changes in the thermo-hydraulic properties of the soil and to infer mechanisms of coupled heat transfer and water vapor flow.

MATERIALS

The physical modeling experiments were performed on a layered system involving a 62-mm-thick layer of Nevada sand having a porosity of 0.43 overlain by a 500-mm-thick layer of unsaturated, compacted Bonny silt having a porosity of 0.47. Nevada sand is classified as SP according to the Unified Soil Classification System (USCS) and a porosity of 0.43 corresponds to a relative density of 60%. Bonny silt is classified as ML (inorganic silt) according to the USCS and has a specific gravity of 2.65. The optimum water content and the maximum dry unit weight corresponding to the standard Proctor compaction effort are 13.6% and 16.3 kN/m^3, respectively. The initial thermal conductivity for compacted Bonny silt under these conditions is approximately 1.2 W/(m·K), although this value is likely to change with variations in degree of saturation and temperature (Smits et al. 2013).

EXPERIMENTAL SETUP AND PROCEDURES

Schematics of the physical models of the SBTES systems fabricated to study coupled heat transfer and water flow in the unsaturated soil layers are shown in Figure 3. The cylindrical aluminum container has a diameter of 603 mm and a height of 554 mm. The base of the container has two ports on opposite sides to permit inflow and outflow of water into the base of the container for control of the water table. One of the ports was connected to a constant-head Mariotte bottle to maintain the water table at the top of the sand layer.

The first step in preparing the physical model was to place a layer of Nevada sand at the bottom of the container using air pluviation. A thin filter fabric was placed over the surface of the sand to prevent its mixing with the overlying silt layer. Next, the silt layer was compacted in seven lifts to achieve a void ratio of 0.90 (porosity of 0.47) that is uniform with depth. Three of U-tubes having an outside diameter of 6 mm and an inside diameter of 2 mm, and a length of 560 mm were buried during the compaction. The distance between the inlet and outlet pipes is approximately 75 mm. The 5TE dielectric sensors for measurement of temperature and volumetric water content and SH-1 thermal needle for measurement of the thermal conductivity of the silt with the KD2Pro system (all obtained from Decagon Devices of Pullman, WA), along with the closed-loop heat exchangers were placed in the silt layer during compaction at the locations shown in Figure 3. The dielectric sensors were placed at a vertical spacing of 85 mm apart along radial center of the soil layer. The thermal needle was placed at mid-height of the silt layer at the center of the container. After all the lifts and sensors were placed in the soil, EL-USB-2LCD relative humidity/temperature sensors manufactured by Lascar Electronics were placed on the soil surface as well as in the same room as the experiment. Next, several layers of plastic wrap were placed on the soil surface to minimize loss of water to the laboratory air due to evaporation. The top and sides of the container were then wrapped in insulation with 2 layers to minimize heat loss from the soil layer. The four type-K thermocouple profile probes, each containing six thermocouples at a spacing of 30 mm) were pushed through the insulation into the compacted silt layer at different radial distances summarized in Table 1.

A schematic of the physical model and the temperature control system is shown in Figure 4. A high-temperature water pump was used to circulate water through a temperature-regulated heated reservoir and into the array of steel closed-loop “U”-tube heat exchangers. The heated reservoir is pressurized to minimize the chances for air bubbles from stopping the operation of the pump under high temperatures. In order to see how much heat is transferred in the soil, pipe plug thermocouples probes (Model TC-J-NPT-G-72 from Omega, Inc.) were also used to measure the temperature of the water going into and out of the heat exchanger tubes. After saturation of the sand layer, heated water was circulated through the heat exchanger pipes. More details of the testing setup are provided in Traore (2013).

RESULTS

Two heat injection tests were performed on identical soil layers with borehole heat exchanger arrays having radial spacings of 80 and 300 mm from the center of the container. Although the dielectric sensors and the thermal conductivity sensor were placed at the same locations in the center of silt layer in both tests, the radial locations of the thermocouple profile probes were different. A summary of the radial distances of the closed loop heat exchanger tubes and the thermal sensor probes in both tests is also shown in Table 1. The entering and exiting temperatures of the water in the borehole heat exchangers are shown in Figures 5(a) and 5(b) for Tests 1 and 2, respectively. At steady-state, the entering and exiting water temperatures were approximately 85 and 80 °C for Test 1, while they were 86 and 79 °C for Test 2. The flow rate of the water circulating through the heat exchanger tubes was 0.38 l/s in both tests, and was assumed to be steady throughout the tests. The slight difference in the temperature difference reflects a greater heat flux into the soil layer in Test 2, for reasons that will be discussed later. However, the heat exchangers had similar average temperatures in both tests.

The temperatures at the surface of the soil layers and within the laboratory are shown in Figures 6(a) and 6(b) for Tests 1 and 2, respectively, while the relative humidity values of the soil surface (beneath the hydraulic barrier) and the ambient laboratory are shown in Figures 6(c) and 6(d) for Tests 1 and 2, respectively. The ambient temperature and relative humidity of the laboratory oscillate on a daily basis due to the operation of the heating and cooling system, while the temperature and relative humidity at the surface of the soil layer beneath the hydraulic barrier and insulation layer reach stable values (50 ºC and 70%, respectively, after 10 hours in Test 1 and 45 ºC and 70%, respectively, after 30 hours in Test 2). To minimize heat loss from the setup, insulation was placed over the hydraulic barrier so only slight oscillations in the room temperature were observed to affect the soil surface temperatures.

The changes in temperature at the depths of the five dielectric sensors installed in the center of the silt layer are shown in Figures 7(a) and 7(b) for Tests 1 and 2, respectively. In both tests, the tests started at an ambient laboratory temperature of 26 °C, and it ranged between 26 and 29 °C. The temperatures at the center of the silt layer reached a stable value after approximately 30 hours of operation for Test 1, but they didn’t reach a stable value until after approximately 60 hours for Test 2. This can be attributed to the wider spacing. The corresponding changes in volumetric water content are shown in Figures 7(c) and 7(d) for Tests 1 and 2, respectively. The volumetric water content values inferred from the dielectric sensors were corrected to account for temperature effects as follows: $\theta_w = \theta_{w,measured} - 0.001725\Delta T$, where ΔT is the change in temperature at the location of each sensor. In Test 1, a brief increase in volumetric water content at the center of the array is observed, after which a steady decrease in water content occurs for the remainder of the test. This occurred as water was initially driven away from the heat exchangers toward the center of the array, after which water was driven outward from the array. In Test 2, a steady increase in volumetric water content at the center of the array is observed. This may have occurred because water loss to the outside of the array was prevented by the container (and thus the array) in Test 2, but also because of the possible formation of a convective cell within the array where water was rising upward from the water table.

The average changes in temperatures with depth from each of the thermocouple profile probes installed at different radial distances from one of the heat exchangers are shown in Figures 8(a) and 8(b) for Tests 1 and 2. As expected, the thermocouple profile probes indicate that temperatures of the soil decrease with radial distance from the heat exchangers. This information is useful for assessment of the thermal conductivity of the soil outside of the array, which will be presented later.

Profiles of temperature with depth along the center of the soil layer are shown in Figures 9(a) and 9(b) for Tests 1 and 2, respectively. In both tests, the smallest temperatures were observed at the bottom and top of the silt layer due to upward and downward heat loss, while the highest changes in temperatures were observed at mid-height. The lower temperatures in the wider borehole array may be due to the greater loss of heat through the boundary of the container due to the contact between the boreholes and the metal heat exchangers. The greater uniformity of temperature with depth in Test 2 have occurred due to the convective mixing within the soil array. Profiles of volumetric water content are shown in Figures 9(c) and 9(d) for Tests 1 and 2, respectively. The water content was relatively uniform with depth in Test 1, and upward water flow due to capillary rise was not observed. In addition to a steady increase in water content in Test 2, the soil closer to the water table was observed to become wetter with time. This is due to both capillary rise and potentially to a greater amount of upward water vapor flow due to buoyancy. Although water was visually observed to condense at the soil surface in both experiments, downward liquid water flow due to gravity was not observed to be significant compared to the rate of upward vapor flow. Longer testing times may have revealed this phenomenon. Alternatively, testing of the small-scale model in a geotechnical centrifuge may help better replicate the roles of capillary rise and downward liquid water flow so that they are more representative of field conditions in a full-scale SBTES system.

The apparent thermal conductivity and specific heat capacity of the unsaturated silt measured using the thermal needle probe embedded at the center of the profile are shown in Figures 10(a) and 10(b) for Tests 1 and 2, respectively. In Test 1, the thermal conductivity at the center of the array was observed to increase up to 1.35 W/(m•K) for a brief period that corresponds to the peak in volumetric water content. After this point, the apparent thermal conductivity of the soil within the array was observed to decrease slowly to a value of approximately 0.55 W/(m•K). The specific heat capacity increases slightly after the volumetric water content starts to decrease, after which it decreases to a value of 1.5 MJ/(m^3•K). This implies that the maximum heat storage within the array decreases over time as the degree of saturation within the array decreases. Different behavior was noted in Test 2. The apparent thermal conductivity was observed to increase slowly throughout the test to a steady value of 1.22 W/(m•K). The specific heat capacity was also observed to increase during the first 220 hours of operation until it reached a steady value of 2.05 MJ/(m^3•K). Post-test evaluation of the gravimetric water content distribution in the soil layer in Test 1 indicates that water in the soil within the array was observed to move outside of the array into the surrounding soil in Test 1. A distinct zone of drying was not observed in the soil layer in Test 2.

ANALYSIS

To analyze the heat transfer and water flow in the vadose zone within the closed-loop heat exchangers array, the coupling between the different thermo-hydraulic properties of the unsaturated soil must be characterized. Relationships between the apparent thermal conductivity, specific heat capacity, temperature, and degree of saturation are shown in the Figure 11. The degree of saturation was calculated from the change in volumetric water content ($\Delta S = S_0 - \Delta\theta/n$, where S_0 is the initial degree of saturation and n is the porosity of the soil). The results indicate the apparent thermal conductivity is sensitive to both degree of saturation as well as temperature (Smits et al. 2013). The specific heat capacity appears to be relatively insensitive to temperature and is more closely related to the degree of saturation.

Although the apparent thermal conductivity of the mass of soil outside of the heat exchanger array was not measured directly, it can be estimated from the average soil temperature values measured using the thermocouple profile probes by assuming that conduction is the mode of heat transfer so that Fourier's law can be used to estimate the thermal conductivity. Specifically the form of Fourier's law governing conductive heat transfer in soil away from a cylindrical heat source is given as follows (Carslaw and Jaeger 1959):

$$\dot{Q} = -2\pi R l \lambda \left[\frac{dT}{dr}\right] \quad (1)$$

where $\dot{Q}$ (W) is the heat transfer rate, λ (W/m K) is the soil thermal conductivity, l (m) is the total length of the borehole, R (m) is the radius of the borehole, and $\left[\frac{dT}{dr}\right]$ (K/m) is the temperature gradient in the soil defined from the thermocouple measurements at different radial locations. The term $2\pi Rl$ (m^2) is the average surface area of a heat exchanger borehole from which heat is transferred. The value of $\dot{Q}$ can be estimated by assuming that convection is the main heat transfer process in the flowing fluid within the array using the following equation:

$$\dot{Q}=\dot{V}_w \rho_w C_w (T_{¿}-T_{out}) \qquad (2)$$

where $\dot{V}$ is the volumetric flow rate of water in ml/s, □$_w$ is the density of water (1 g/ml), C_w is the specific heat capacity of water equal to 4183 J kg^{-1} K^{-1} , and T_{in} and T_{out} are the temperatures of the water entering and exiting the heat exchanger loops, respectively. The equation for the apparent thermal conductivity of the soil outside of the array can be estimated by combining Equations (1) and (2), as follows:

$$\lambda=\frac{\dot{V}\rho C (T_{¿}-T_{out})}{-2\pi Rl\left[\frac{dT}{dr}\right]} \qquad (3)$$

The apparent thermal conductivity of the soil outside of the heat exchanger array in Test 1 can be compared with that of the soil within the heat exchanger array, as shown in Figure 12. It is clear that the apparent thermal conductivity of the soil outside of the borehole heat exchanger array increased during the test, likely due to the gradual wetting of the soil due to thermally-induced water flow out of the array. Although this comparison was not possible for Test 2 as the heat exchangers were located at the edge of the container, the comparison for Test 1 confirms the importance of considering thermally induced water flow on the heat transfer processes in SBTES systems in the vadose zone.

The results in Figure 10 and 11 confirm that the thermal conductivity is closely related to the degree of saturation. Thermally-induced water flow will lead to an increase in apparent thermal conductivity of the soil, leading to an increase in heat transfer into the soil. For Test 1 (80 mm array spacing) the degree of saturation decreases at a change in temperature of 31 ºC, leading to a corresponding decrease in apparent thermal conductivity. The heat transfer within the heat exchanger array causes water to flow out of the soil within the array in the form of water vapor. As a result, the soil pores within the array are filled with air, which is a poor heat conductor. Conduction becomes the main mode of heat transfer within the borehole heat exchangers array, and heat transfer into the array decreases. Different from the results in Test 1, the presence of the extra water due to thermally-induced water flow and capillary rise within the array in Test 2 led to a sustained increase in apparent thermal conductivity in the soil layer.

A comparison of the change in the degree of saturation at the center of the soil layers in Tests 1 and 2 is shown in Figure 13. A decrease in the degree of saturation within the array in Test 1 occurred as water was permanently driven from the center of the array, which means that this spacing may be too small to induce a convective cell within the array. In Test 2, after the degree of saturation reached a steady value, the thermal conductivity was observed to continue increasing. This is further evidence that a convective cell may have formed within the array.

For simplicity of comparison of the tests in this study, the soil volume within the array is defined as the soil within the radius of the heat exchangers. This definition is necessary as the array with wider spacing in Test 2 is surrounded by a no-flow boundary. However, it differs from the definition of the array for a SBTES system in the field, which will incorporate some of the soil outside of the array itself because this heat can still be accessed during heat extraction (Baser and McCartney 2015). Nonetheless, the heat transferred into the array as a function of time can be estimated using Equation (2). The heat transfer is expected to be initially transient until the soil reaches a constant temperature and water flow ceases. The transient process may be nonlinear due to the effects of thermally induced water flow in the soil. At large times, it is expected that the amount of heat injected will equal the amount of heat lost from the array as the soil has reached is heat capacity. The rate of heat loss from the array in Test 1 can also be estimated using Equation (1), considering the temperature gradient between the array and the soil outside of the array. The thermal conductivity of the soil outside of the array calculated from Equation (3) can be used in the heat loss calculation in the case of Test 1. The rate of heat loss from the array in Test 2 is different due to the presence of the insulated container adjacent to the heat exchangers. In this case, the steady state heat loss rate from the container can be estimated as follows (Gabrielsson et al. 2000):

$$\dot{Q}=\frac{\square_{cont}A_{cont}\left(T_g-T_a\right)}{d} \qquad (4)$$

where $\dot{Q}$ is rate of heat loss from the container (W), $\square_{cont}$is the thermal conductivity of the container (W/(m•K)), A_{cont} is the surface area of the container sides (m^2), d is the thickness of the container, T_g represents the boundary temperature of the array (K), and $T_a$the mean temperature at the outer wall of the container (K). The boundary temperature is assumed to be equal to the mean temperature of the soil within the array and a reasonable estimation of T_a is the mean temperature of the ambient air.

The rates of heat injection and heat loss from the arrays in Tests 1 and 2 are presented in Figure 14(a) and 14(b), respectively. In both tests, the heat injection rate initially has a high value as the temperature gradient between the heat exchangers and the relatively cool soil is high. The heat injection rate then drops over time as the temperature within the array increases until reaching a relatively constant value after approximately 30 hours for Test 1 and after 60 hours for Test 2. The spike in heat transfer rate in Test 1 occurred as the circulation pump shut off accidentally for a moment. The gradual increase in the heat loss from the array in Test 1 is associated with the thermally induced water flow out of the array, making this soil more conductive to heat. The rate of heat loss from the array in Test 2 is steady as the temperature of the soil and the outside of the container were relatively constant during the test. At steady state, it is clear that more heat is transferred to the unsaturated silt within the array in Test 2 than in Test 1. This is primarily due to the greater amount of soil to be heated within the array in Test 2, but may be due partially to the enhanced thermal properties of the unsaturated soil associated with convective processes.

In either test, the heat storage can be defined with energy balance within the array corresponds to the difference in the cumulative amounts of heat injected into the soil and the amount of heat lost from the array, which can be defined as follows:

$$Q_{stored} = Q_{injected} - Q_{lost} \quad (5)$$

The cumulative heat injection and loss along with the corresponding heat storage in Tests 1 and 2 are shown in Figures 15(a) and 15(b). The total heat storage in Test 1 is observed to initially increase due to the transient effects at the beginning of the test, but is then observed to decrease due to the steady heat injection at the same time as the increase in heat loss. Due to the high heat loss, the heat storage appears to tend toward a maximum value of 253 MJ. The heat storage in

Test 2 also initially increases steeply, but after 60 hours increases at a steady rate after approximately 60 hours. Although the soil reached a steady temperature and water content profile, the heat storage did not reach a stable value, possibly due to inaccuracies in calculating the temperature gradient across the container wall in Equation 4. The results from the tests are summarized in Table 2. Despite the different durations of the two tests, they were performed until the water flow within the array stabilized. Despite the difference in durations, a greater amount of heat had been injected into the array in Test 2 after 30 hours of heating (the time when Test 1 was stopped), which can be attributed to the role of coupled heat transfer and water flow in this test, and potentially the formation of a convective cell in the array.

CONCLUSIONS

The role of coupled water and heat transfer in unsaturated soil layers was assessed in this study to better understand the behavior of soil-borehole thermal energy storage (SBTES) systems installed in the vadose zone. The results from two tests involving three closed-loop heat exchangers at radial spacing of 80 and 300 mm in the 500 mm-thick layer of unsaturated silt are reported, which provide useful information for the validation of thermo-hydraulic flow simulations. In each test, water with a temperature of approximately 80 °C was circulated through the heat exchangers to inject heat into the unsaturated soil layer. In both tests, the apparent thermal conductivity was observed to depend on the degree of saturation of the soil and the temperature. For the borehole array with the smaller spacing, permanent drying of the soil within the array was observed shortly after heating started. A convective cell was not formed in this array, and heat transferred into the array was observed to decrease over time as the soil dried. Further, the rate of heat loss from the borehole array to the surrounding soil was observed to increase with time as thermally induced water flow away from the array carried more heat out of the array than into the array. For the borehole array with the larger spacing, the soil layer experienced an increase in water content over time, indicating superior heat transfer due to coupling between water flow and heat transfer. The soil within the array with wider spacing was observed to steadily increase in degree of saturation and thermal conductivity, which corresponds to the greater rate of heat injection in this test. A slight increase in the specific heat capacity was also observed. The heat storage, defined as the difference between the cumulative amounts of heat injected and lost from borehole array, was greater in the array with larger spacing where outward water flow was prohibited by the container. Not only was there a larger zone of soil, but the rate of heat was greater in the array with a larger spacing. This occurred as there was a larger zone of soil within the array and because the soil experienced a greater increase in water content within the area during heating due to coupled heat transfer and water flow into the array.

ACKNOWLEDGEMENTS

Funding provided by NSF grant 1230237 is much appreciated. The opinions in this paper are those of the authors alone.

REFERENCES CITED

Başer, T. and McCartney, J.S., 2015, Development of a full-scale soil-borehole thermal energy storage system, Proceedings of the International Foundations Conference and Equipment Exposition. San Antonio, TX. Mar. 17-21. ASCE. p. 1-10.

Carslaw, H.S. and Jaeger, J.C., 1959. Conduction of Heat in Solids. Oxford Clarendon Press, 2^{nd} edition, 517 p.

Cass, A., Campbell, G.S., and Jones, T.L., 1984, Enhancement of thermal water vapor diffusion in soil, Soil Science Society of America Journal, 48:25-32.

Gabrielsson, A., Bergdahl, U., and Moritz, L., 2000, Thermal energy storage in soils at temperatures reaching 90°C,Journal of Solar Energy Engineering, 122:3-8.

Lu, N., 2001, An analytical assessment on the impact of covers on the onset of air convection in mine wastes, International Journal for Numerical and Analytical Methods in Geomechanics, 25:347-364.

McCartney, J.S., Ge, S., Reed, A., Lu, N., and Smits, K., 2013, Soil-borehole thermal energy storage systems for district heating, European Geothermal Congress, Pisa, June 3-7, 1-10 (CD-ROM).

Sakaguchi, I., Momose, T., and Kasubuchi, T., 2007, Decrease in thermal conductivity with increasing temperature in nearly dry sandy soil. European Journal of Soil Science. v. 58, p 92–97, doi:10.1111/j.1365-2389.2006.00803.

Sibbitt, B., Onno, T., McClenahan, D., Thornton, J., Brunger, J., Wong, B., 2007, The Drake Landing Solar Community project – Early results, Canadian Solar Buildings Conference, Calgary, June 10-14, 1-8 (CD-ROM).

Sibbitt, B., McClenahan, D., Djebbara, R., Thornton, J., Wong, B., Carriere, J., and Kokko, J., 2012, The performance of a high solar fraction seasonal storage district heating system - Five years of operation, Energy Procedia. 30: 856–865.

Smits, K.M., Sakaki, T., Howington, S.E., Peters, J.F. and Illangasekare, T.H., 2013, Temperature dependence of thermal properties of sands over a wide range of temperatures [30-70ºC], Vadose Zone Journal, doi:10.2136/vzj2012.0033.

Traore, T., 2013, Physical Modeling of Coupled Water and Heat Flow within a Borehole Heat Exchanger Array in the Vadose Zone, MS Thesis, University of Colorado Boulder, 147 p.

Zhang, R., Lu, N., and Wu, Y.-S., 2012, Efficiency of a community-scale borehole thermal energy storage technique for solar thermal energy, Proceedings of GeoCongress 2012, ASCE, pp. 4386-4395.

FIGURE CAPTIONS

Figure 1. Mechanisms of heat transfer and water flow within a convection cell formed within an array of geothermal heat exchangers in the vadose zone

Figure 2. Heat transfer and water flow processes in the vadose zone within the context of the boundary conditions representative of SBTES systems

Figure 3. Elevation and plan views of the soil container showing instrumentation and expected heat transfer processes in the physical model (note: one heat exchanger is shown out of plane in the elevation views for emphasis): (a) Small array; (b) Large array

Figure 4. Schematic of the overall experimental setup

Figure 5. Inlet and outlet fluid temperatures: (a) Test 1; (b) Test 2

Figure 6. Temperature and relative humidity at the soil surface (under the hydraulic barrier) and in the laboratory (a) Temperature in Test 1; (b) Temperature in Test 2; (c) Relative humidity in Test 1; (d) Relative humidity in Test 2

Figure 7. Time series of dielectric sensor data: (a) Change in temperature in Test 1; (b) Change in temperature in Test 2; (c) Change in volumetric water content in Test 1; (d) Change in volumetric water content in Test 2

Figure 8. Change in average soil temperatures with depth at different horizontal distances from the center of the borehole heat exchanger array: (a) Test 1; (b) Test 2

Figure 9. Profile data from the dielectric sensors embedded in the center of the soil layer at different depths: (a) Change in temperature in Test 1; (b) Change in temperature in Test 2; (c) Change in volumetric water content in Test 1; (d) Change in volumetric water content in Test 2

Figure 10. Time series from the thermal conductivity sensor embedded in the middle of the unsaturated soil layer: (a) Test 1; (b) Test 2

Figure 11. Pictures of the excavated soil layer after heating: (a) Test 1; (b) Test 2

Figure 12. Apparent thermal conductivity, specific heat capacity, and degree of saturation with the change in temperature at the center of the borehole array: (a) Test 1; (b) Test 2

Figure 13. Comparison of thermal conductivity inside and outside the borehole array in Test 1

Figure 14. Degree of saturation as a function of borehole heat exchanger spacing

Figure 15. Heat transfer rates: (a) Test 1; (b) Test 2

Figure 16. Evaluation of the energy balance: (a) Test 1; (b) Test 2

Table 1. Details of the physical modeling tests on SBTES systems with different array spacings

Test	Dry density	Initial volumetric water content	Initial degree of saturation	Porosity	Borehole array radial spacing	Radial locations of thermocouple profile probes			
						r_1	r_2	r_3	r_4
	(kg/m^3)	(m^3/m^3)	(m^3/m^3)	(m^3/m^3)	(mm)	(mm)			
1	1400	0.236	0.40	0.47	80	110	160	210	260
2	1400	0.233	0.40	0.47	300	300	250	200	150

Table 2. Summary of the estimated heat transfer and heat storage calculations for both tests

Test	Spacing	Duration until reaching stable water content	Average steady-state heat transfer	Average steady-state heat loss	Total heat injected	Total heat lost	Total heat stored
	(mm)	(hours)	(W)	(W)	(MJ)	(MJ)	(MJ)
1	80	435	646	555	873	620	253
2	300	715	975	399	2364	915	1449

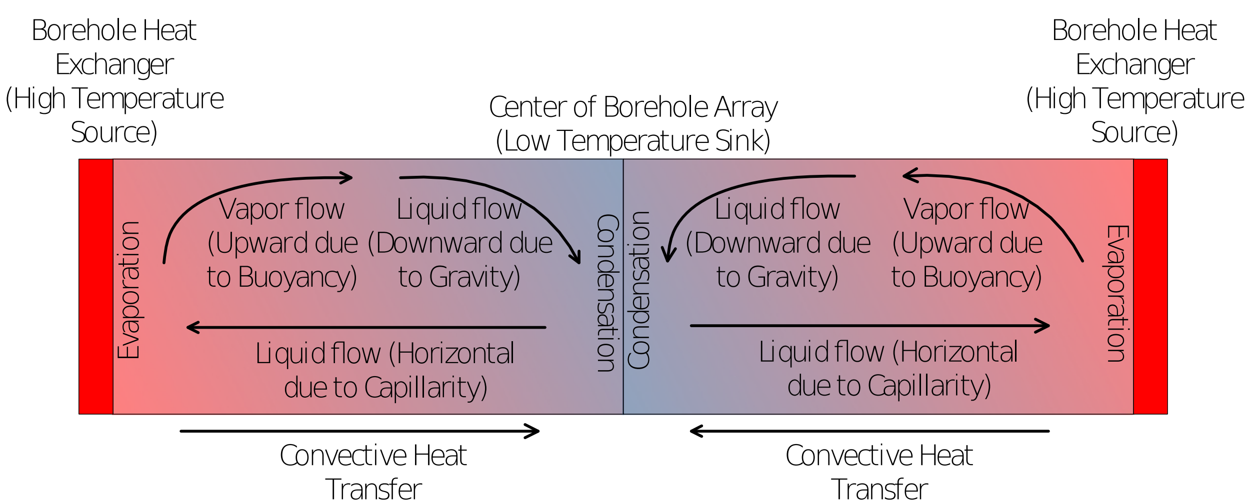

Figure 1. Mechanisms of heat transfer and water flow within a convection cell formed within an array of geothermal heat exchangers in the vadose zone

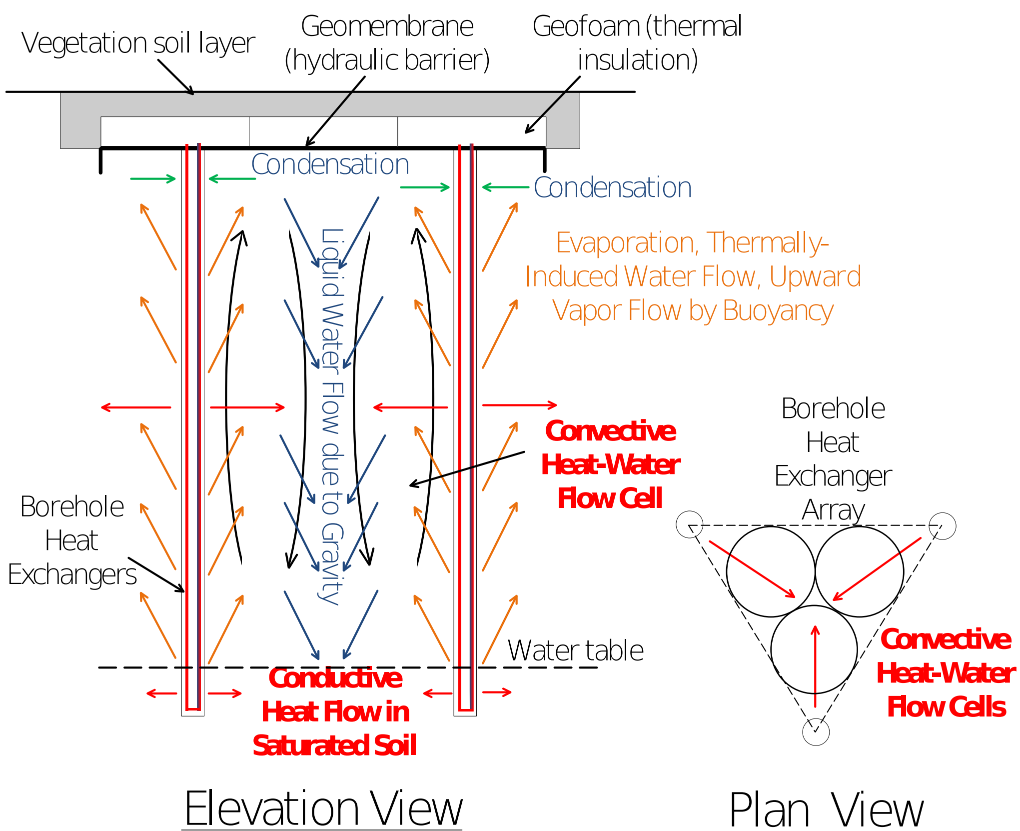

Figure 2. Heat transfer and water flow processes in the vadose zone within the context of the boundary conditions representative of SBTES systems

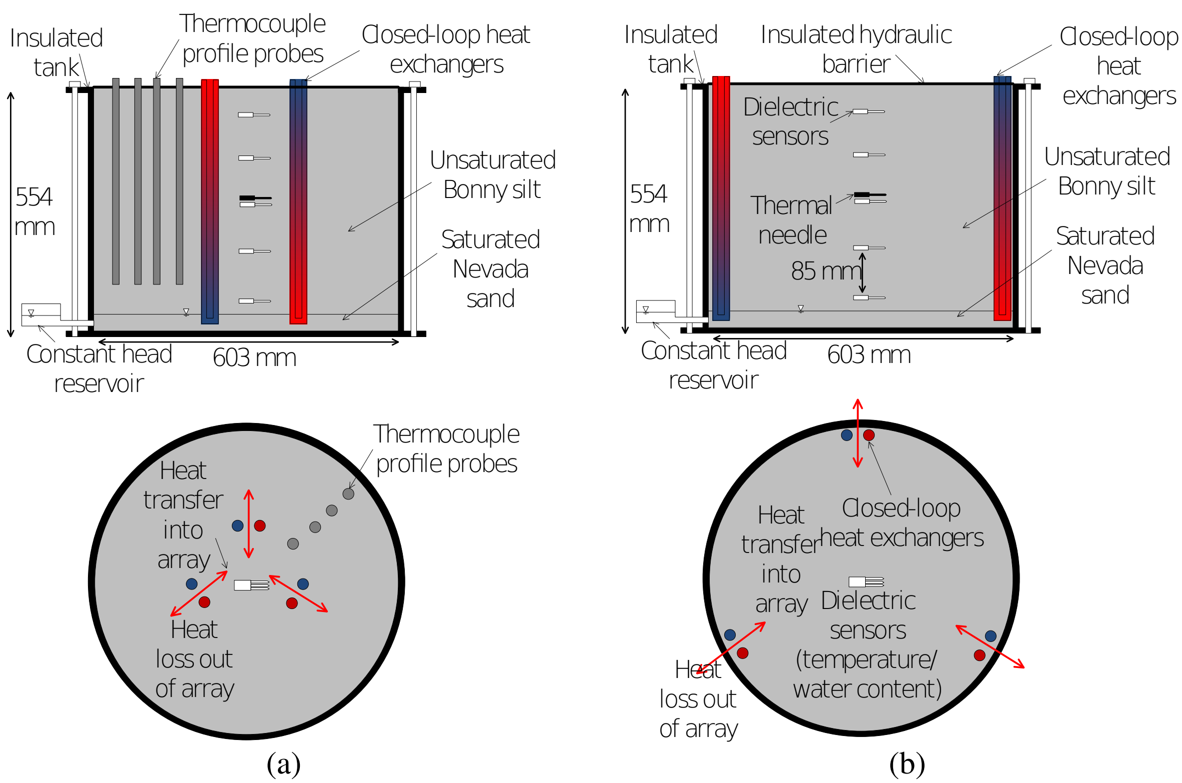

Figure 3. Elevation and plan views of the soil container showing instrumentation and expected heat transfer processes in the physical model (note: one heat exchanger is shown out of plane in the elevation views for emphasis): (a) Small array; (b) Large array

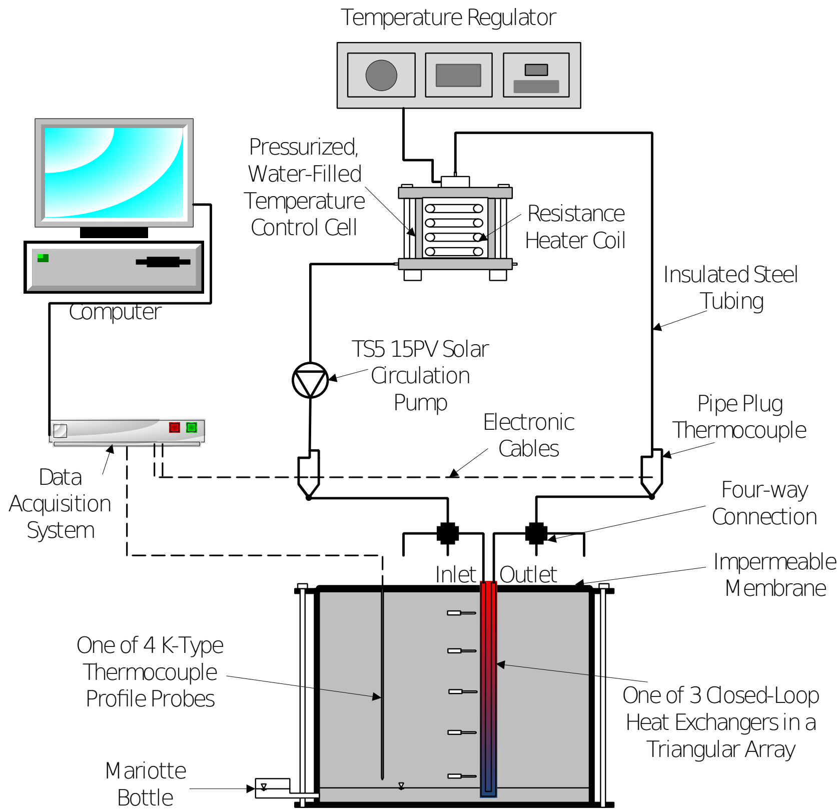

Figure 4. Schematic of the overall experimental setup

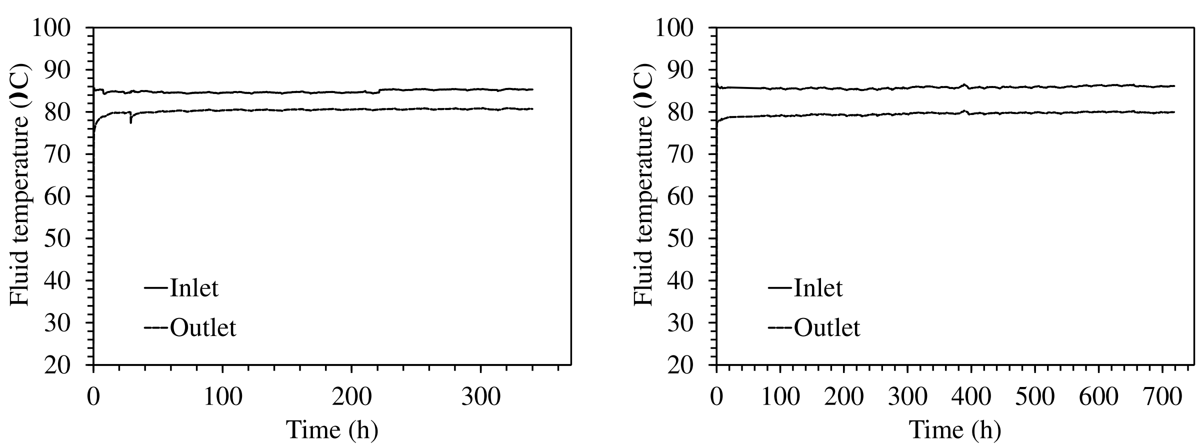

(a) (b)

Figure 5. Inlet and outlet fluid temperatures: (a) Test 1; (b) Test 2

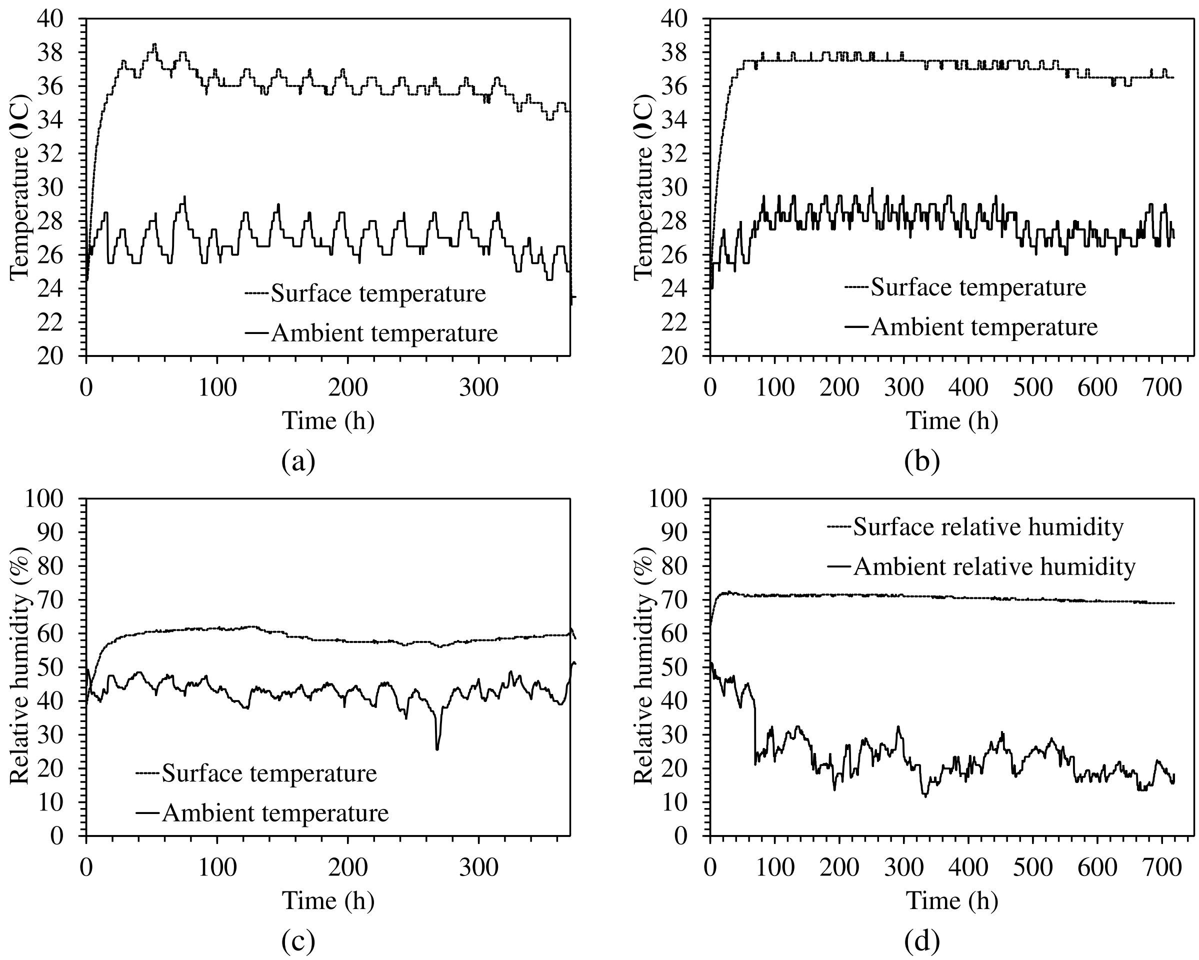

Figure 6. Temperature and relative humidity at the soil surface (under the hydraulic barrier) and in the laboratory (a) Temperature in Test 1; (b) Temperature in Test 2; (c) Relative humidity in Test 1; (d) Relative humidity in Test 2

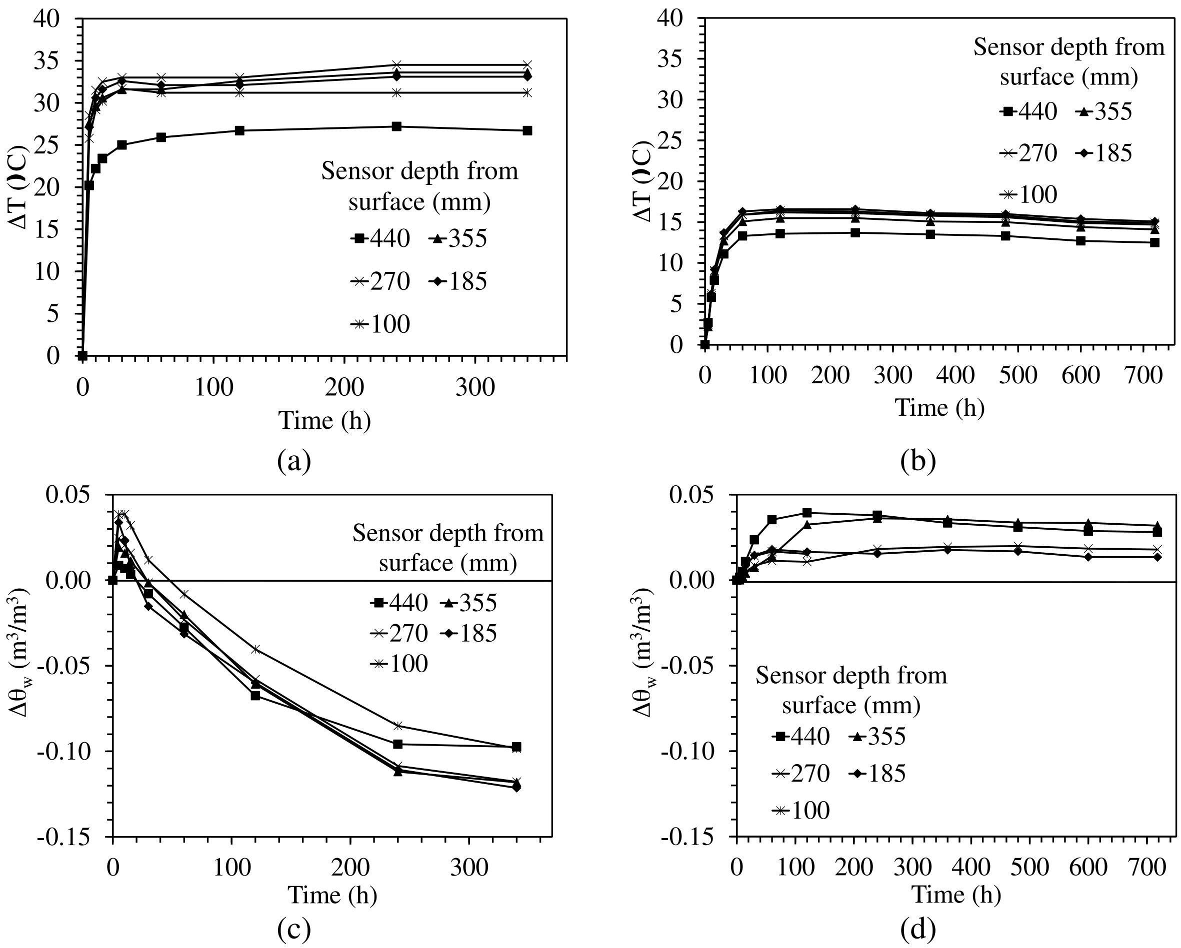

Figure 7. Time series data of dielectric sensor embedded in the middle of soil at different depths: (a) Change in temperature in Test 1; (b) Change in temperature in Test 2; (c) Change in volumetric water content in Test 1; (d) Change in volumetric water content in Test 2

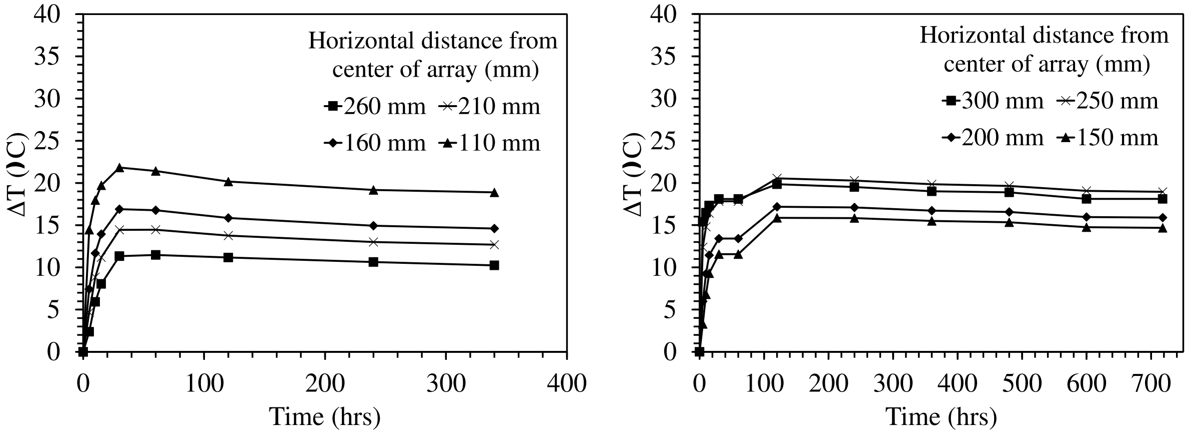

(a) (b)

Figure 8. Change in average soil temperatures with depth at different horizontal distances from the center of the borehole heat exchanger array: (a) Test 1; (b) Test 2

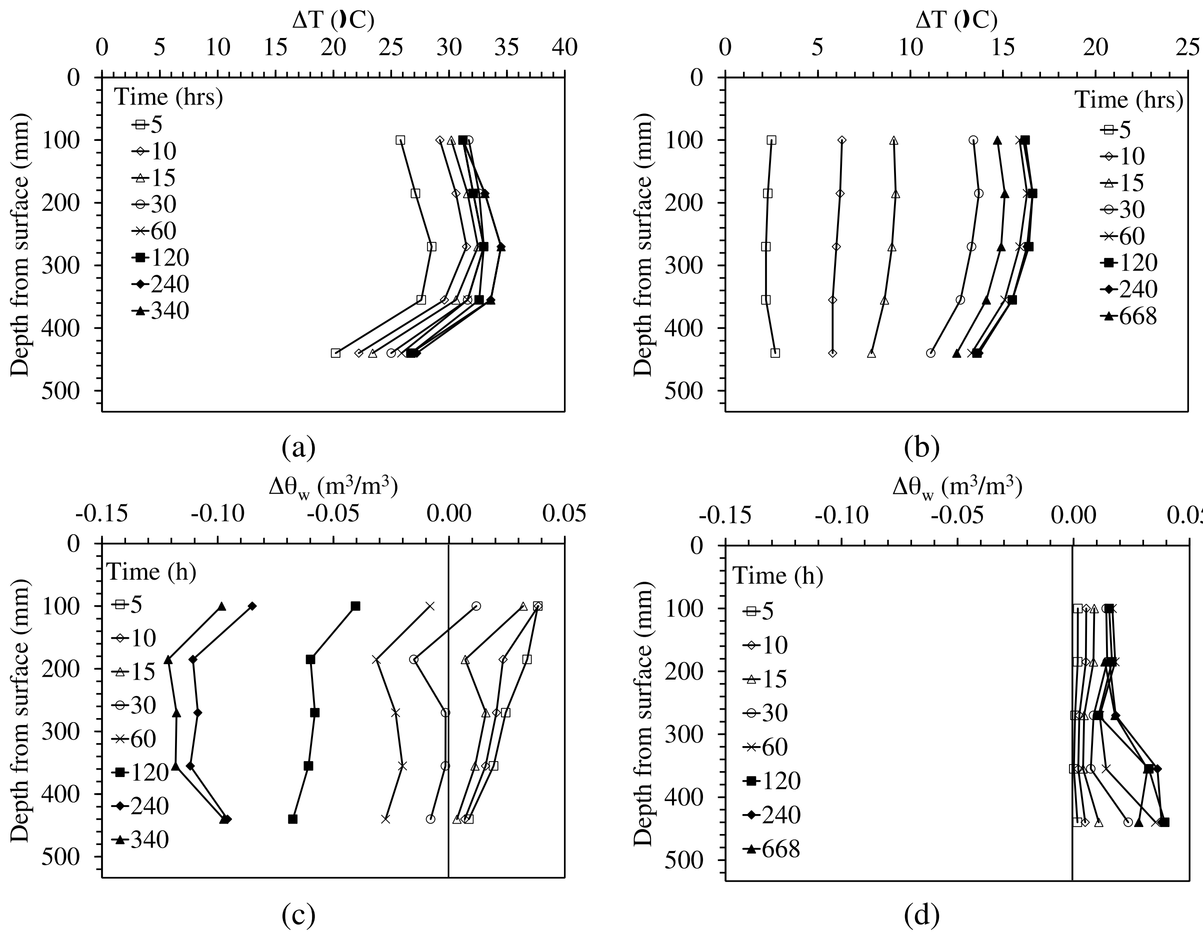

Figure 9. Profile data from the dielectric sensors embedded in the center of the soil layer at different depths: (a) Change in temperature in Test 1; (b) Change in temperature in Test 2; (c) Change in volumetric water content in Test 1; (d) Change in volumetric water content in Test 2

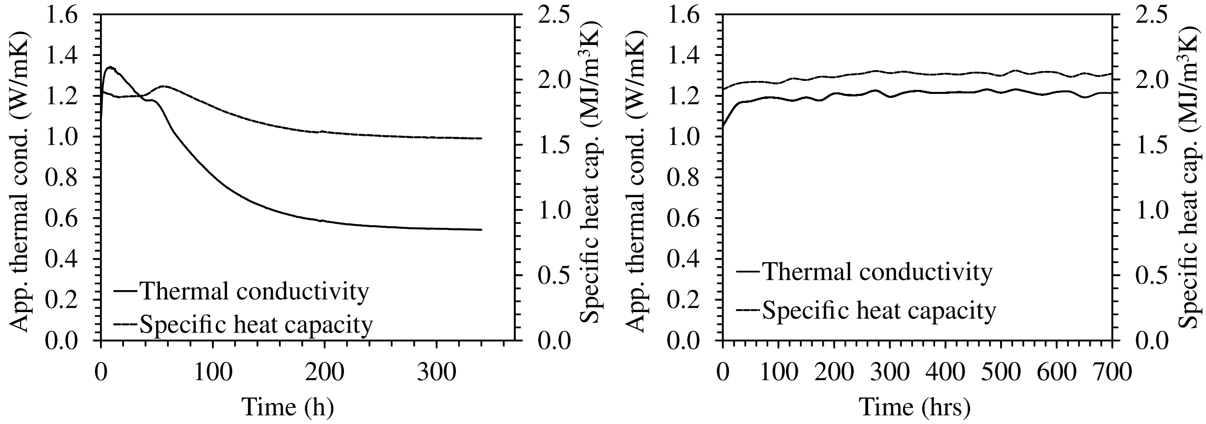

(a) (b)

Figure 10. Time series from the SH-1 thermal sensor embedded in the middle of the unsaturated soil layer: (a) Test 1; (b) Test 2

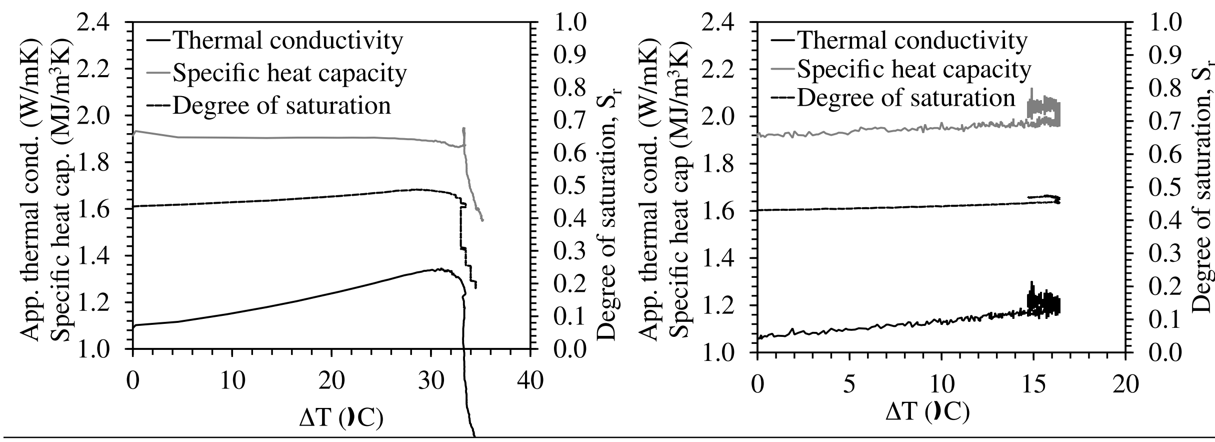

(a) (b)

Figure 11. Apparent thermal conductivity, specific heat capacity, and degree of saturation with the change in temperature at the center of the borehole array: (a) Test 1; (b) Test 2

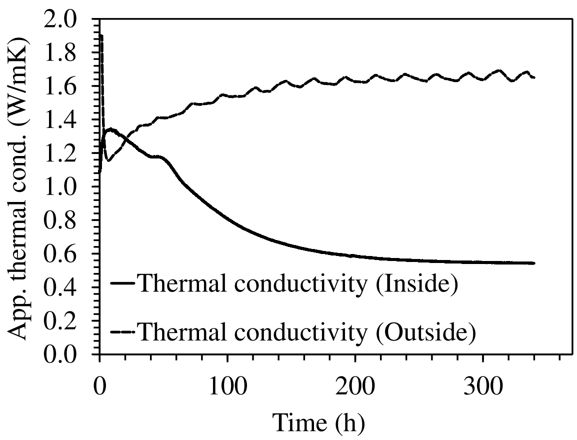

Figure 12. Comparison of the soil thermal conductivity inside (from thermal conductivity sensor) and outside (from Fourier's analysis) the borehole array in Test 1

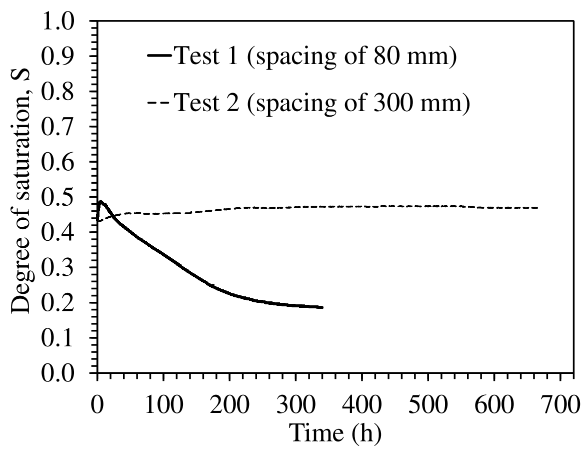

Figure 13. Degree of saturation as a function of borehole heat exchanger spacing in Tests 1 and 2

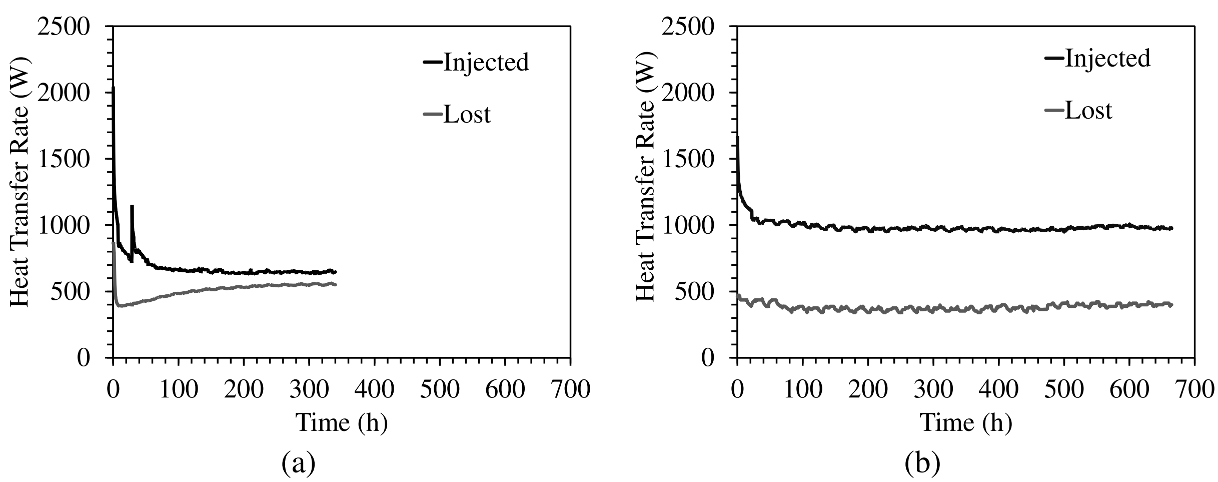

Figure 14. Heat transfer rates: (a) Test 1; (b) Test 2

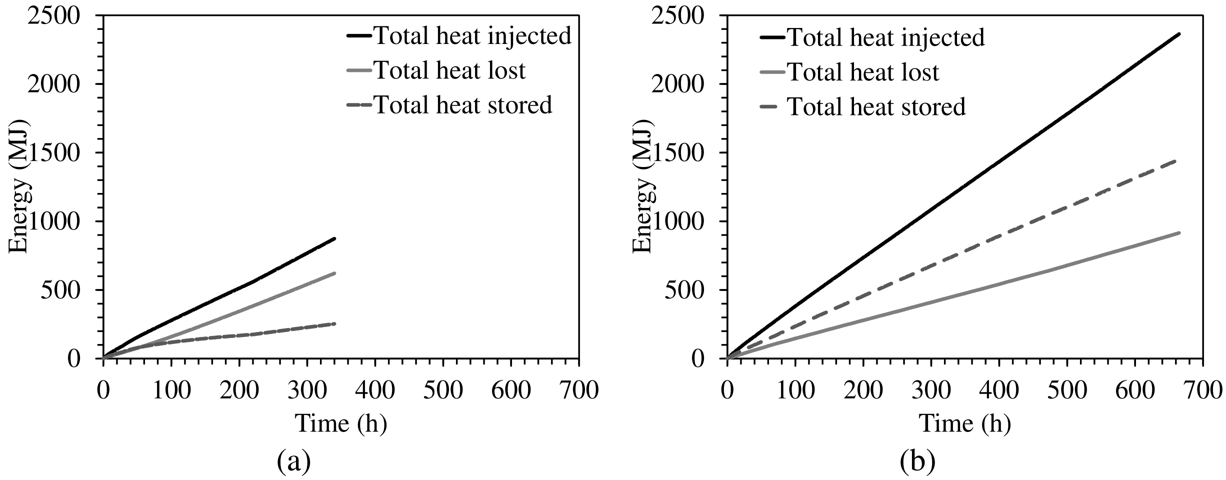

Figure 15. Evaluation of the energy balance: (a) Test 1; (b) Test 2